Bidirectional DEM relief shading method for extraction of gully shoulder line in loess tableland area

Jiaming Na, Xin Yang, Wen Dai, Min Li, Liyang Xiong, Rui Zhu & Guoan Tang

Published online: 05 Dec 2017.

Submit your article to this journal ⌃

Article views: 138

View related articles ⌃

View Crossmark data ⌃

Citing articles: 1 View citing articles ⌃

Taylor & Francis
Taylor & Francis Group

Check for updates

Bidirectional DEM relief shading method for extraction of gully shoulder line in loess tableland area

Jiaming Na[a] , Xin Yang[a], Wen Dai[a], Min Li[b], Liyang Xiong[c], Rui Zhu[d] and Guoan Tang[a]

[a]Key Laboratory of Virtual Geographic Environment, Ministry of Education, Nanjing Normal University, Nanjing, China; [b]Jiangsu Centre for Collaborative Innovation in Geographical Information Resource Development and Application, Nanjing Normal University, Nanjing, China; [c]State Key Laboratory Cultivation Base of Geographical Environment Evolution, Nanjing Normal University, Nanjing, China; [d]Department of Land Surveying and Geo-Informatics, Hong Kong Polytechnic University, Hong Kong, Hong Kong

ABSTRACT

The gully shoulder line, one of the most important topographical features, reveals the erosional process and reflects the geomorphological evolution of a loess area. Existing shoulder-line extraction methods are based on local window-filter or image-edge detection, which are sensitive to image noises and algorithm parameters, causing unsatisfactory accuracy and efficiency. This paper proposes a bidirectional relief-shading (BRS) method for loess shoulder-line extraction based on a 5-m Digital Elevation Model (DEM). First, two hill-shaded images are simulated with appropriate altitude and symmetric direction of the light. Second, the grey value difference between inter-gully and inner-gully area can be easily identified by fusing the two images with the mean method. Finally, the shoulder line can be derived by image segmentation using a threshold determined by an empirical equation. Experiments in three areas of loess tableland in Shaanxi Province validated the method, which has the advantages of being a simple operation with relatively high accuracy, 89.7% compared with manual digitalization, and high efficiency. We discuss three parameters in this method: zenith angle, azimuth angle, and segment threshold. Results suggest that the method is applicable for broad-scale gully shoulder line extraction in loess tablelands.
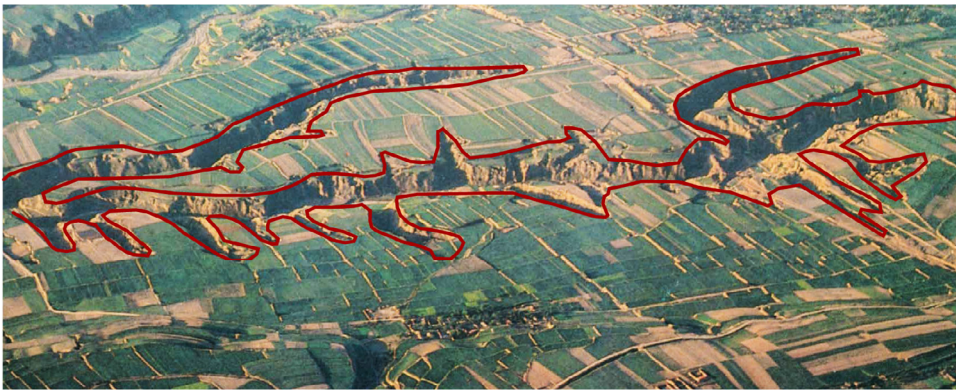
Introduction

Soil erosion is a serious environmental problem that causes land degradation and natural hazards, especially in loess plateau areas in China (Wang, Zheng, Römkens, & Darboux, 2013). The shoulder line, as the boundary of a gully area (red line in Figure 1(a)), is widely used for monitoring and predicting gully erosion and gully development (Castillo & Gómez, 2016; Li, Zhang, Zhu, He, & Yao, 2015; Noto, Bastola, Dialynas, Arnone, & Bras, 2017; Shruthi, Kerle, Jetten, Abdellah, & Machmach, 2015). The shoulder line, as a critical terrain structural line, separates inter-gully (BC) and inner-gully areas (AC) (Figure 1(b)), namely,

---

Figure 1. (a) Shoulder line in a typical gully system in loess plateau of China; (b) Illustration of a typical terrain profile near the loess shoulder line, which is the boundary between inter-gully and inner-gully areas (Yan et al., 2014).

the positive and negative terrains (P-N terrain) attributed to surface and gully erosion, respectively (Yan, Tang, Li, & Zhang, 2014). The shoulder line also partitions different land uses. The area above the shoulder line generally has a gentle slope and is usually cultivated for agriculture, while the area below the shoulder line is characterized by a steep slope with intense soil loss, and is usually left as barren land (Chen & Cai, 2006). Mapping loess shoulder lines provides gully morphologic information for research on gully erosion (Li et al., 2017), landscape development (Qiu et al., 2010), and land-use change (Jiang, Tang, & Liu, 2015; Poesen, Nachtergaele, Verstraeten, & Valentin, 2003).

Manual digitalization by field survey, topographic maps, or remote sensing images has been extensively used for shoulder-line delineation, but has high temporal and pecuniary cost, especially for a large area. With the development of remote sensing techniques and GIS-based spatial analysis in recent years, many methods have been designed to extract shoulder lines automatically based on Digital Elevation Models (DEMs). They can be categorized into terrain morphologic feature methods and image gradation detection methods.

Terrain morphologic feature-based methods delineate the locations of loess shoulder lines by analyzing statistical attributes of the DEM, such as slope (Tang, Xiao, Jia, & Yang, 2007), aspect (Lv, Qian, & Chen, 1998), curvature (Zhu, Tang, Zhang, Yi, & Li, 2003), and flow accumulation (Liu et al., 2016). Implementation of terrain morphologic feature-based methods can be accomplished easily, using local neighborhood analysis. However, a discontinuous shoulder line would be generated by this local window analysis, due to the morphologic complexity of the shoulder lines. Some global analysis methods, such as the Hilditch algorithm (Li, Wang, & Li, 2008), hydrological analysis (Zhou, Tang, Wang, Xiao, et al., 2010; Zhou, Tang, Yang, Xiao, et al. 2010), and principal component analysis (PCA) (Chen et al., 2012), have been introduced in loess shoulder-line extraction. All of these methods can obtain candidate points of the shoulder line in a certain density by window filter-based analysis so that a series of points can be connected in sequence to construct a complete shoulder line. However, the size of the window filter obviously influences the accuracy of the result, which means that a local analysis window could hardly achieve a satisfactory accuracy at a global perspective. Wang, Wang, Zhang, and Ding (2015)_ENREF_12 proposed a new method using global terrain openness and threshold segmentation instead of local window-filter analysis. Their method is scale-free and can obtain high spatial accuracy, but has low computational efficiency. In summary, terrain morphologic feature-based methods are sensitive to scale of the analysis window, resulting in low accuracy although they are easily implemented.

Image gradation detection methods use an edge-detection algorithm to obtain the shoulder line based on the grey scale variation of elevation or terrain parameters (e.g. slope) derived from a DEM. Yan, Tang, Li, and Dong (2011) employed the Laplacian of Gaussian (LoG) detector to extract loess shoulder lines after a comparison of four different edge detectors. Then, an integrating algorithm of a hydrological D8 algorithm and Snake model were proposed (Yan et al., 2014; Zhou, Tang, Xi, & Tian, 2013). Since more topographic parameters are taken into consideration besides DEM elevation, the results of image gradation detection methods achieve relatively higher accuracy. However, more complex extraction procedures reduce the efficiency and limit their application for large areas. Song et al. (2013) developed the Gradient Vector Flow (GVF) method, a parallel version of the Snake model. The accuracy of GVF is still not satisfied, although the computational efficiency increases significantly. Moreover, shoulder lines obtained from these methods are too smooth to reflect the complex morphology of gullies realistically, and the parameters of these methods rely on specific geomorphologic features of the study area, which makes application transformation difficult.

The hillshade model, also called shaded relief, is an advanced technique for terrain visualization based on light simulation. It can achieve continuous color or grey-scale output by simulating solar radiation on a terrain (Horn & Schunck, 1981). The stereoscopic sense could be promoted significantly by using this model, but few studies have applied this model to geomorphologic research, particularly for terrain feature extraction. Some studies have adopted a hillshade model for landslide mapping (Barbier, Proisy, Véga, Sabatier, & Couteron, 2011; Van Den Eeckhaut et al., 2005). Chen et al. (2012) used the data-mining method of PCA to obtain the P-N terrains, and this method is based on a designed multivariate statistics index named "multi-azimuth DEM shaded relief and slope." This is the first time that a hillshade model was used for shoulder line extraction, but the procedure is relative complex. Inspired by their work, we propose a relative simple method for shoulder-line

extraction with acceptable accuracy in the area of loess tableland named "bidirectional relief-shading method" (BRS method). Our method consists of three major steps: (1) to simulate hillshade images in a bidirectional orientation, (2) to overlay and generate a mean value image of these two hillshade images, and (3) to segment the image into two parts, as positive and negative terrain, using a threshold determined by an empirical equation. The objectives of this paper are: (1) to develop a simple method for loess shoulder-line extraction; (2) to present the parameters used in the test area, and (3) to assess the performance of this method in both accuracy and efficiency.

Methods

Shoulder-line extraction based on bidirectional DEM shaded relief

The DEM shaded relief method is usually applied to calculate the relative radiation value of each grid cell and is represented by illumination or grey scale. The commonly used formula (Yoëli, 1967) is:

$$E = E_0 \times \left(\cos(\theta_z) \times \cos(\emptyset_s) + \sin(\theta_z) \times \sin(\emptyset_s) \times \cos(\theta_A - \emptyset_A) \right) \tag{1}$$

where E_0 is the maximum brightness, and the default value is 255; θ_z is the zenith angle, namely, the angle between local normal and illumination direction, which is the 90° complement to the altitude angle; θ_A is azimuth angle, which is the direction of the illumination source; $\emptyset_A$ is the aspect degree of the terrain surface; and $\emptyset_s$ is the slope degree of the terrain surface. For each specific terrain surface, $\emptyset_A$ and $\emptyset_s$ are determined by the local terrain.

Figure 2 shows the transverse profile of a gully in a loess tableland area characterized by much flat terrain surface, in which deep-cut gullies developed. The inner-gully area (the area below the shoulder line) usually has a steep slope, while the inter-gully area (the area above shoulder line) is usually flat or has a very gentle slope. When illuminating terrain surfaces with an ideal light source (optimal θ_A and θ_z), one side of the gully area will be shaded. If the light source is reversed, the other side of the gully area will be shaded (Figure 2(a)). When two hill-shading maps are averaged, the grey values of the resulting image would be much different on different sides of the shoulder line. Generally, the value is much higher on a sunny slope (inter-gully area above shoulder line) than on a shaded slope (inner-gully area below shoulder line). Therefore, the shoulder line can be extracted by separating terrain surfaces into two regions according to the difference in grey values of hill-shading images.

The zenith θ_z and azimuth θ_A of the light source are the two key parameters for shoulder-line extraction in this method. For example, the lower zenith θ_z may produce a non-shaded area in the gully bottom, resulting in a faulty shoulder line in the inner gully area (Figure 2(b)). With a higher θ_z, all gully area will be shaded (Figure 2(c)). In addition, the number of directions that is enough for shoulder-line extraction should be explored because gullies in a large area may extend in multiple directions. We designed two experiments to detect the optimal value. The workflow is shown in Figure 3, and key procedures for shoulder line extraction are described in the following sections.
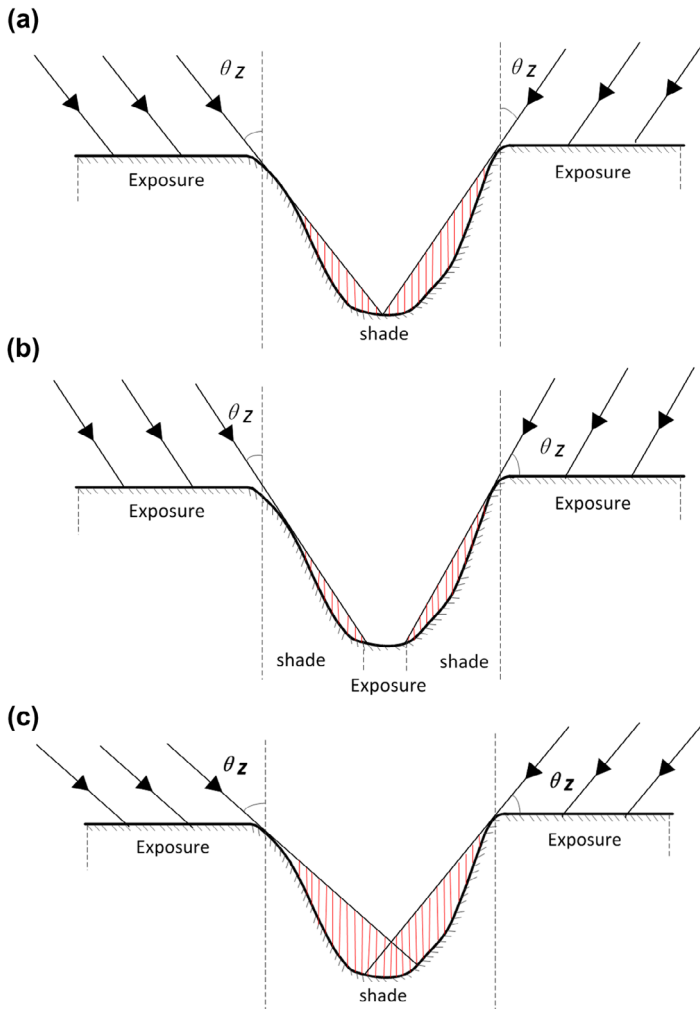
Figure 2. Illustration of sunlight illumination on a gully area. (a) the basic idea of BRS, (b) with a lower zenith θz, (c) with a higher θz.
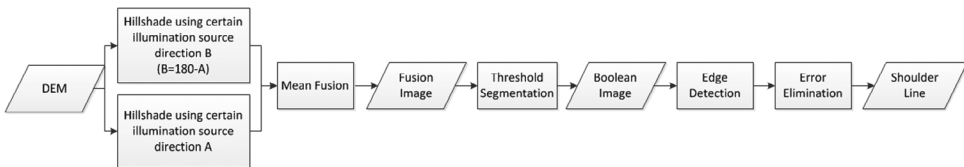

Figure 3. Workflow of the proposed BRS method.

Select appropriate zenith angle of light source

Given that the cross section of the loess gully is generally U- or V-shaped (Figure 2(a)), a shaded-relief simulation of these two symmetric directions could reflect the significant difference between positive and negative terrains on both sides of a gully. To make all of the gully area be shaded, the zenith angle of light, θ_z, should be greater than the complementary

angle of the average slope of the inter-gully area, i.e. the average slope in the area above the shoulder line (Figure 2(a)). Several gully profiles were sampled for testing the range of θ_z. The optimum θ_z is within the overlapped scope of all zenith ranges of sample gullies (Figure 4).

Select the appropriate azimuth angle of light source

Considering that the positive terrain in a loess tableland is almost flat, hill-shading images simulated from any azimuth direction θ_A are substantially similar, i.e. bright in flat areas and dark in the gully area. However, the result may be different if the gully's direction is just the same or parallel to the direction of the simulated light. Therefore, three pairs of directions, i.e. NE-SW, SE-NW, and SSE-NNW, are selected to explore the influence of azimuth angle. The optimum θ_A can be determined by comparing the extracted results with the reference data.

Hillshade calculation and threshold segmentation

After calculating the mean brightness of two hill-shading images, a significant difference can be observed between the inter-gully and inner-gully areas, i.e. positive and negative terrains in the entire area. Image segmentation can overcome the local discontinuity of extracted shoulder lines. By employing a proper global threshold t, we can achieve a reasonable result when dividing the loess terrain into positive and negative surfaces with polygon features:

$$R = \begin{cases} 1 & (E < t) \\ 0 & (E \geq t) \end{cases} \tag{2}$$

where E is the mean brightness, R is the reclassification result, and t is the segmentation threshold. $R = 1$ denotes inner-gully area or negative terrain, and $R = 0$ indicates inter-gully area or positive terrain. A visual comparison between the segmentation results and the reference data (or image) could be used to determine the optimized value of t. Notice that t varies with different values of θ_z. We found a linear relationship between θ_z and t. Thus, t can be determined accordingly once the optimum θ_z has been determined. This result will be discussed in detail in Section 'Segmentation threshold'.
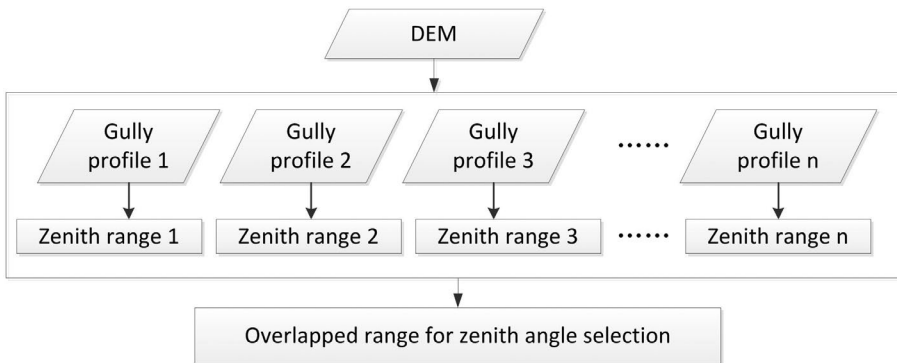

Figure 4. Zenith angle selection.

Error elimination

If some holes or sinks still exist in the segmentation results due to local terrain relief complexity or data noises, a minor revision is necessary. In this process, some isolated and minor mistakes (holes with area <500 m^2) are automatically eliminated by a neighborhood analysis (i.e. the Eliminate tool in ArcMap 10.2), and the shoulder line retains as its origin. Notice that some of the area in the flat bottoms of wide gullies may mistakenly be divided into inter-gully area, which will result in "gully bottom lines." When extracting the shoulder line, we delete these lines manually.

Accuracy and efficiency assessment

An indicator, Euclidean Distance Offset Percentage (EDOP), was employed to compare the results with reference data (Jiang et al., 2015). The reference data were the shoulder line, obtained by manual digitalization of a 1-m digital orthophoto map (DOM). The Euclidean distance raster layer (EDRLσ) with a certain distance σ (e.g. 5, 10, and 20 m) to the manual digital shoulder line could be then calculated. After that, extracted shoulder lines (convert the extracted line into raster data) are intersected with the EDRLσ. The pixel located in the EDRLσ could be considered to be correct, and the accuracy could be assessed by calculating the proportion of the correct pixels out of the total pixels of extracted shoulder line, namely, the EDOPσ accuracy. The larger the EDOPσ, the higher the accuracy of the extraction will be. Previous research with the same area and data achieved a high EDOP$_{20}$ (Song et al., 2013); therefore, the EDOP$_{20}$, 20-m buffer zone of the reference data can be used for accuracy assessment. It can also be used for a comparison of our BRS method with Song's methods. The efficiency assessment could be evaluated by the execution time in the same calculation environment (Figure 5).
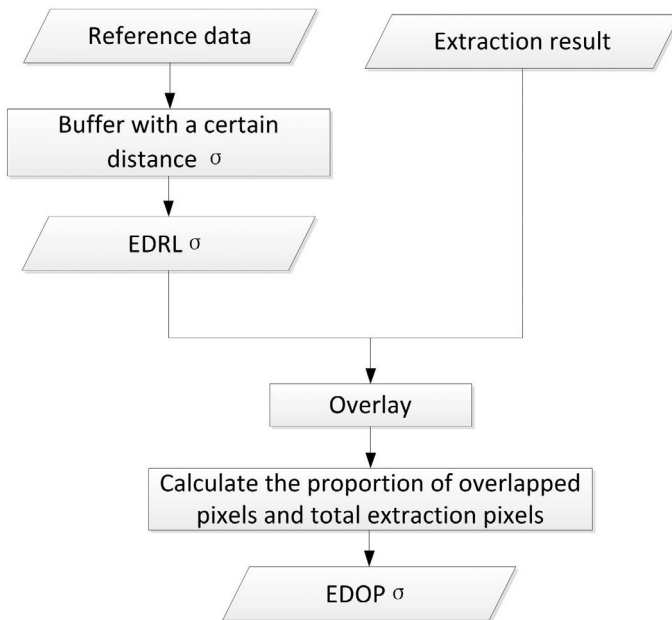

Figure 5. Workflow of the accuracy assessment.

Two other methods, including a terrain morphologic feature method, namely, the P-N method (Tang et al., 2007), and an image gradation detection method, namely, the GVF method (Song et al., 2013), were selected for the comparison with our method in both position accuracy and computation time.

Data and materials

Three areas (Yijun, Chunhua, and Luochuan) in the Loess Plateau of China were chosen to test the performance of the proposed shoulder-line extraction method. Those areas are representative of loess tableland landforms because they are characterized by a relatively broken land surface eroded by thousands of steep gullies. The overall loess tableland is fractured into several separated blocks, resulting in the existence of finger-like loess shoulder lines.

A complete watershed was selected to assess the performance of our BRS method and compare it with other methods. The actual shoulder line was mapped by manual digitization as the reference data (red line in Figure 6(a)). The main gully of this watershed is 6.8 km in length.

All DEMs with 5-m resolution and DOMs with 1-m resolution were used for the experiment. The DEMs were generated by the interpolation of digital contours from a relief map at 1:10,000 scale. Both DEMs and DOMs were provided by the National Administration of Surveying, Mapping, and Geo-information of China.

Results

In TA1, four transverse profiles from four different gullies were sampled randomly to explore the optimal zenith angle (Figure 7). As mentioned in Section 'Shoulder-line extraction based on bidirectional DEM shaded relief', we calculated the average slope of each gully slope through terrain profiling. After overlaying all of them, the average slope of gully side ranged from 26.9° to 48.1°, and the zenith (the complement angle) should be within the range of 41.9° to 63.1°. We selected 45° as the zenith angle for the hillshade simulation.

We also tested the impact of different azimuth angles on the shoulder-line extraction. Our results showed that azimuth angle has a very weak influence on the result (discussed in Azimuth angle). Thus, we used the NE-SW bidirectional pair (135°, 315°) for the hillshade simulation. The results are shown in Figure 8(a) and (b).

For parameter t, after a comparison with the manual reference data, we used a mean fusion operation to determined threshold t for fusion image segmentation. This operation is based on the equation:

$$t = \mu + 0.5\sigma \tag{3}$$

where μ is the mean grey value of the hillshade fusion image and σ is the standard deviation (Figure 8(c)). A threshold t of 167 was obtained by the above equation. Interestingly, we also found a strong linear relationship between θ_Z and t, which will be discussed in segmentation threshold in discussion section. Finally, errors of uncertainty, such as the existence of small blocks and slight discontinuities, were addressed and eliminated (Figure 8(d)). The white areas at the bottom of the inner-gully were deleted manually. Loess gully shoulder lines were then extracted (Figure 9(a)).
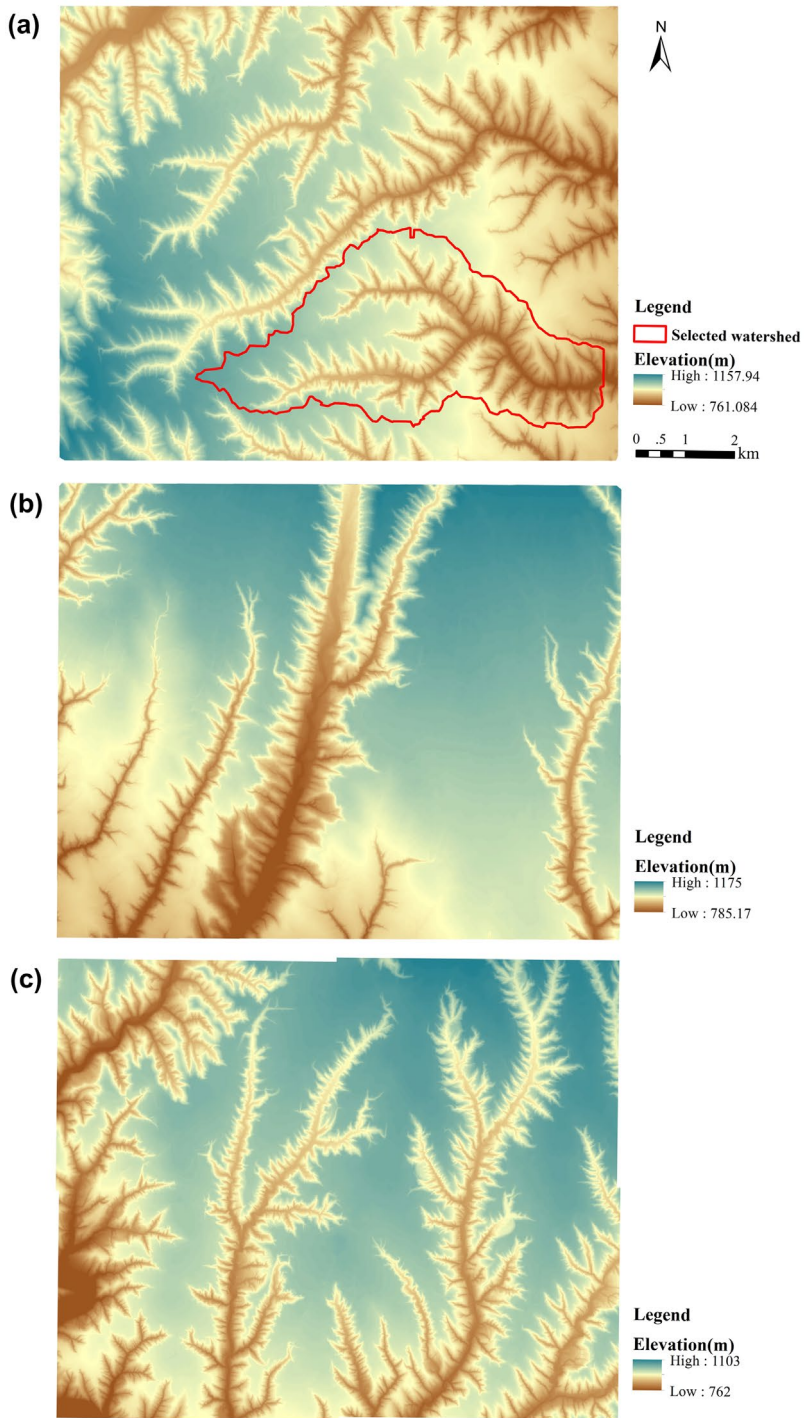
Figure 6. Study area: (a) Yijun (TA1), (b) Chunhua (TA2), and (c) Luochuan (TA3).

Figure 9(a) illustrates the final extraction results of TA1. An overall visual assessment showed that our results have relatively high accuracy and efficiency. The BRS method was performed in other two areas, TA2 (Figure 9(b)) and TA3 (Figure 9(c)) with the same pair
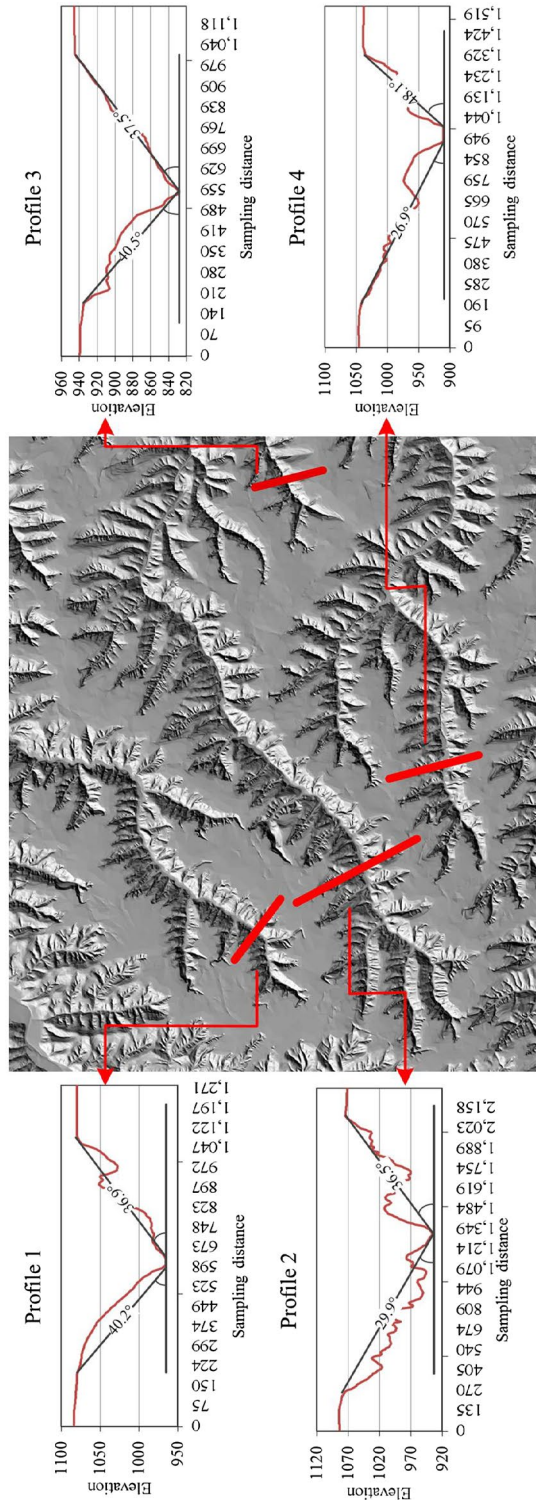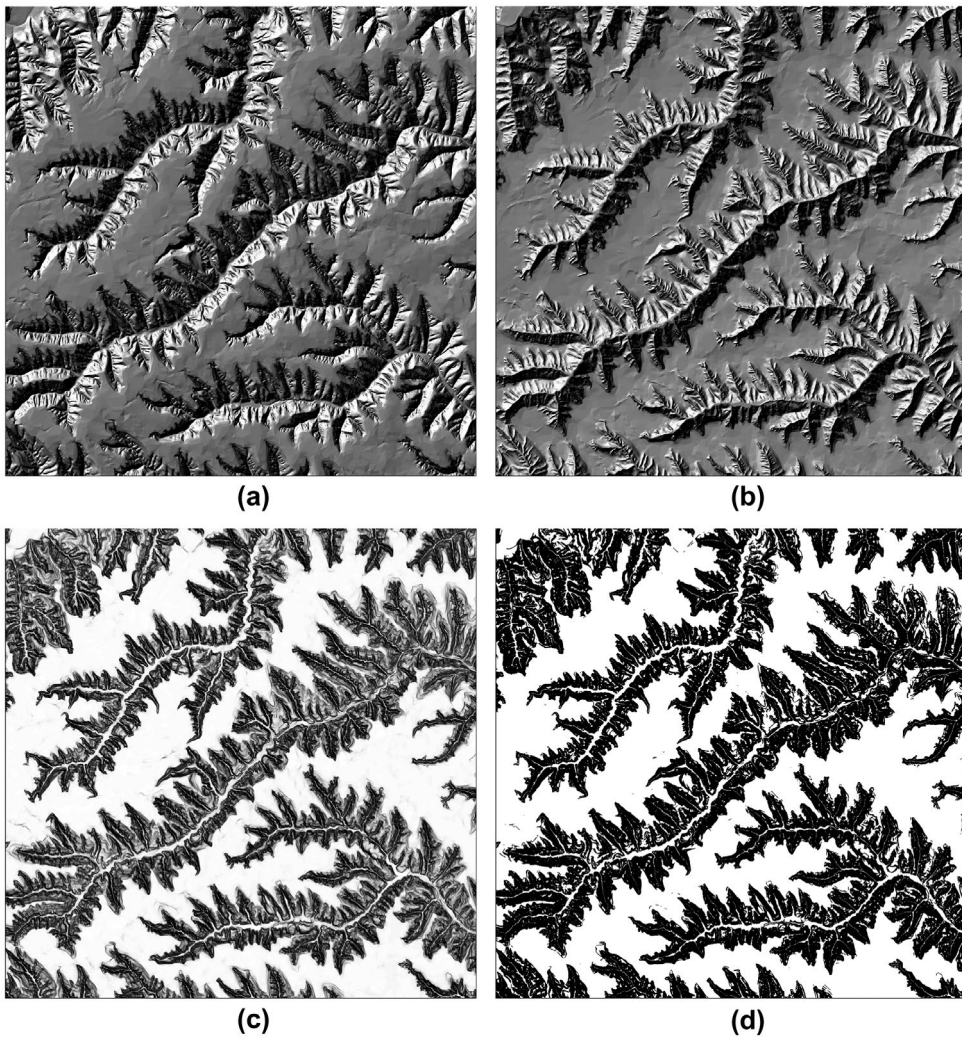
Figure 7. Terrain profiles.

Figure 8. Loess shoulder-line extraction in TA1. (a) Hillshade simulation result using $\theta_A = 315°$, $\theta_z = 45°$; (b) hillshade simulation result using $\theta_A = 135°$, $\theta_z = 45°$; (c) mean fusion result; and (d) segmentation result.

of θ_A (135°, 315°), different values of θ_z (35° in TA2 and 40° in TA3, which were determined by a terrain profile measurement process as mentioned above), and their corresponding t obtained by Equation (3). The extraction results of these two areas confirm a relative strong robustness of the parameter determination method.

Discussion

Azimuth angle

The extraction results of the selected catchment in TA1 using different pairs of bi-directions θ_A – (135°, 315°), (45°, 225°), and (165°, 345°) – are shown in Figure 9(a–c). The parameter
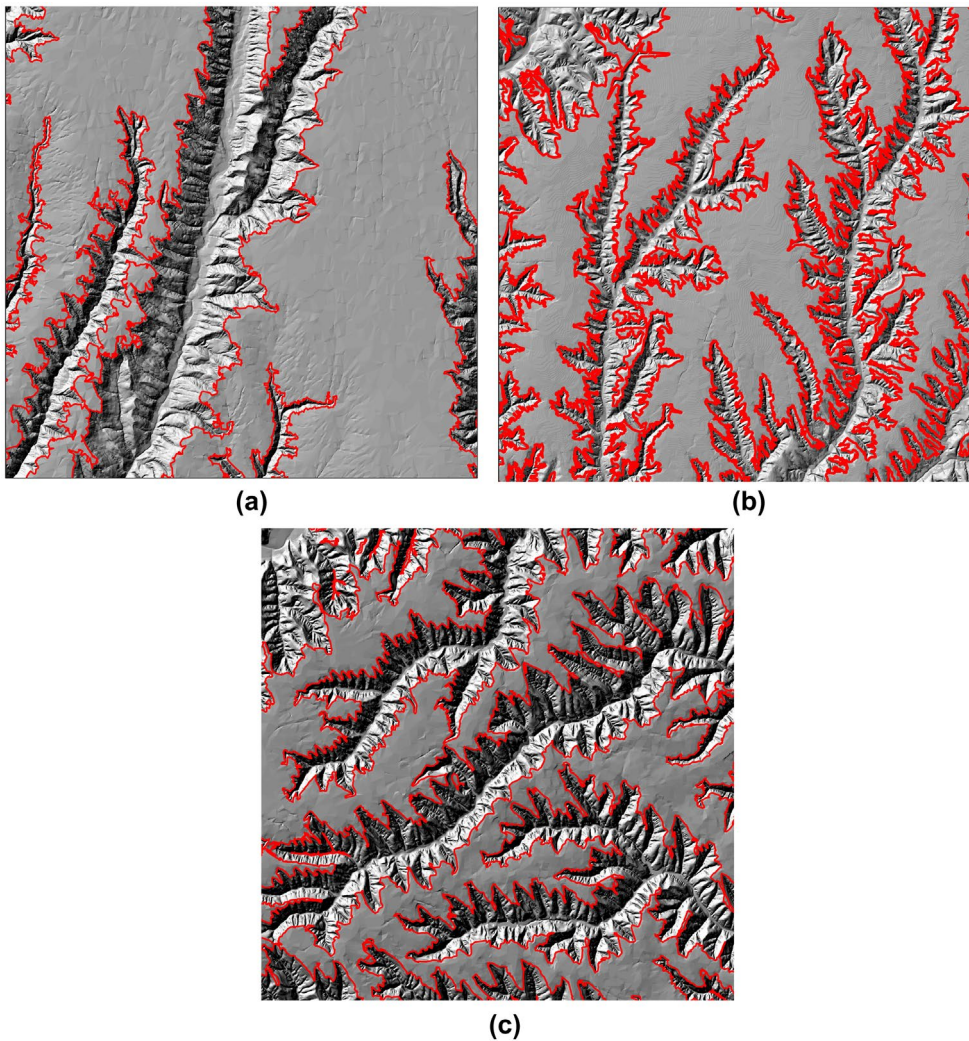
Figure 9. Extraction results for (a) TA1 (Yijun), (b) TA2 (Chunhua), and (c) TA3 (Luochuan).

θ_A was found to have a relatively weak influence on shoulder-line extraction because any azimuth would result in a high value in the flat inter-gully area and much lower value in the steep slope, shaded area (inner-gully area) in the landform of loess tableland. Therefore, the azimuth could be determined easily. In this paper, 135° and 315° were selected as the bidirectional illumination source orientations because they are the most commonly used directions when simulating shaded relief images. If a landform, such as those in loess hilly areas, is more fragmented and complex, with numerous gullies in various directions, additional illumination source directions may be required to ensure that all inner-gully areas could be shaded in the hill-shade image. This will be conducted in future work.
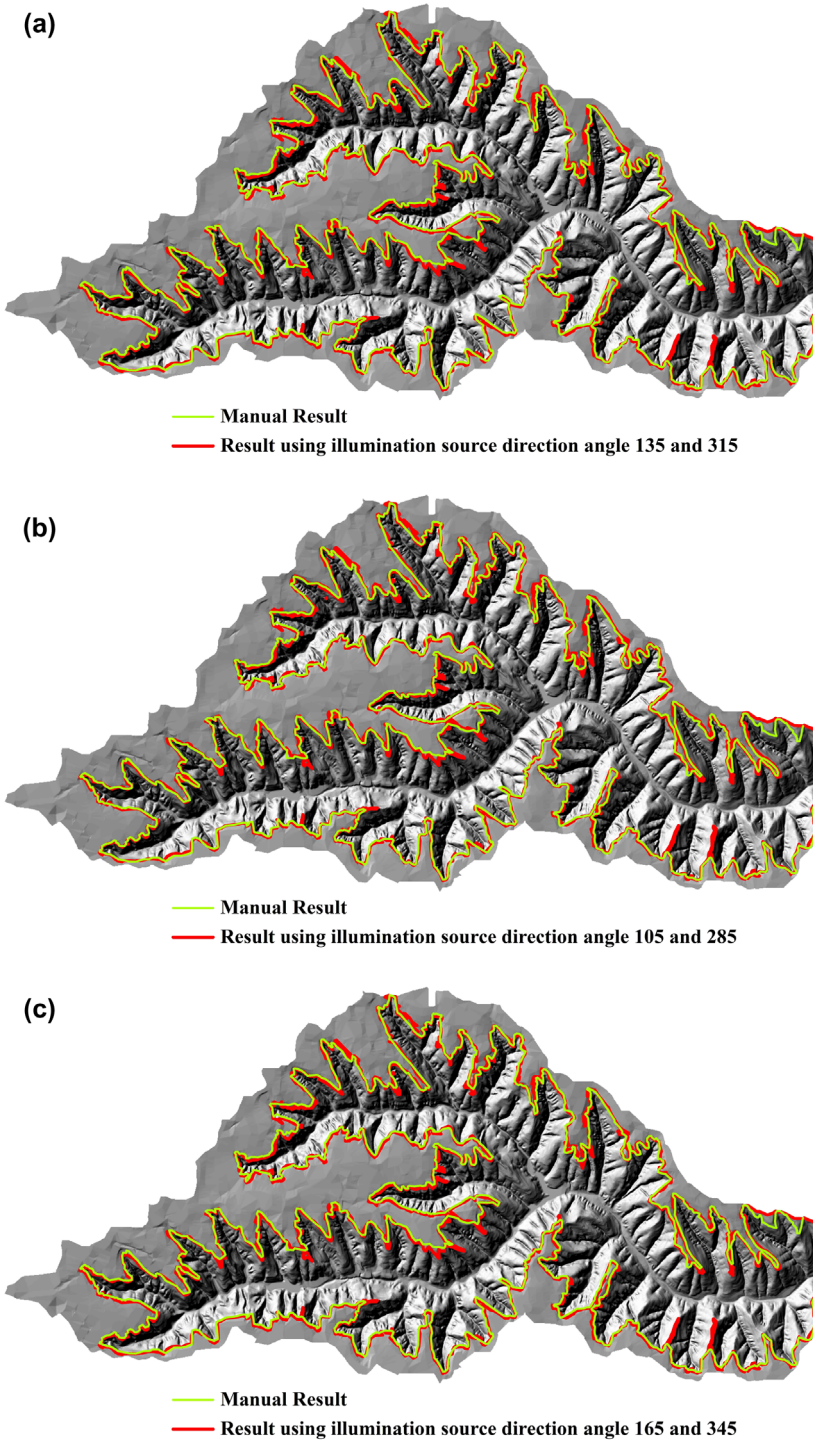
(a)

— Manual Result
— Result using illumination source direction angle 135 and 315

(b)

— Manual Result
— Result using illumination source direction angle 105 and 285

(c)

— Manual Result
— Result using illumination source direction angle 165 and 345

Figure 10. Results using different parameters: (a) $\theta_A = 135°$, $315°$, $\theta_z = 45°$; (b) $\theta_A = 105°$, $285°$, $\theta_z = 45°$; (c) $\theta_A = 165°$, $345°$, $\theta_z = 45°$; (d) $t = 114.5$ (Equal Interval); (e) $t = 151$ (Natural Break); and (f) $t = 178$ (Standard Deviation).

(d)

—— **Manual Result**

(e)

—— **Manual Result**
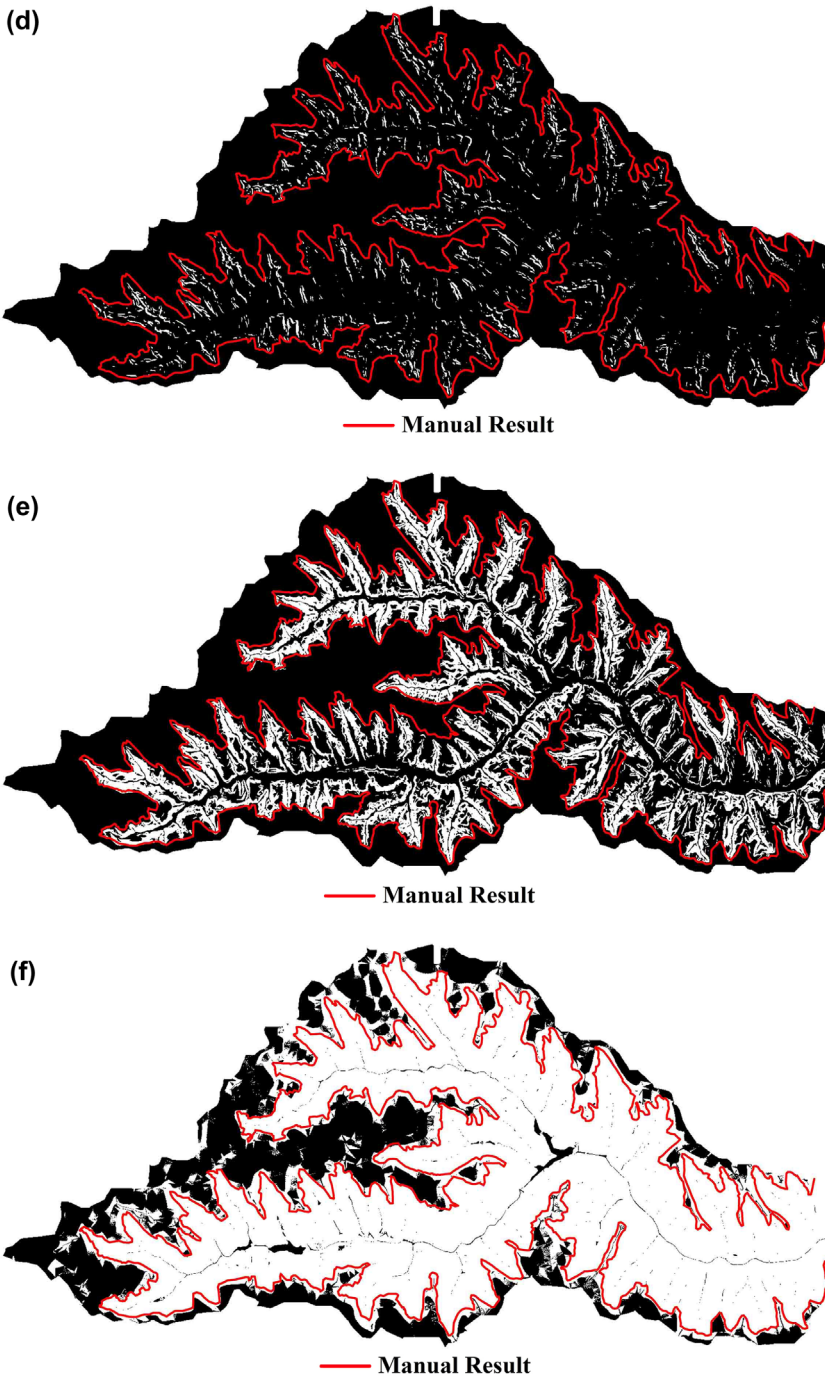
(f)

—— **Manual Result**

Figure 10. (*Continued*).

Segmentation threshold

The image segmentation threshold, *t* in our method, significantly influences the continuity of the shoulder line in both shape and position accuracy. The threshold *t* could be calculated by several generally used methods, such as the Equal Interval method (Figure 10(d)), the Natural Breaks (Jenks) method (Jenks & Caspall, 1971; Figure 10(e)), or the Standard Deviation method (Figure 10(f)). These methods are provided by ArcGIS software. We used these methods to classify the image into a binary one. Then, the shoulder lines were generated by extracting the boundary of the white value area. A comparison with reference data shows that the result obtained by the Natural Breaks (Jenks) method was a bit under-segmented and the method from Standard Deviation was over-segmented. Finally, we found that the optimum threshold of *t* could be acquired by Equation (3), and the results from the other two test areas verified the validity of this equation.

As discussed above, the appropriate zenith angle exists within a range of angles that can be determined by gully transverse profiles. Any angle within this range would be appropriate. However, the fusion images vary slightly for different zenith angles, resulting in different segmentation thresholds. Therefore, we investigated the relationship between the zenith angle and the segment threshold in the TA1 study area. The average and standard deviation value could be quantified by calculating the hill-shading image with a certain zenith angle. Different zenith angles result in different statistical indices, such as average and standard derivation value. Therefore, the *t* value (Equation (3)) has a strong relationship with the zenith angle. To investigate this relationship, we sampled zenith angles from 0° to 90° at 5° intervals and calculated the corresponding *t* values. The scatter plot (Figure 11) shows a strong linear relationship between these two parameters:

$$t = 2.5715\theta_z + 43.571 \ (R^2 = 0.97) \tag{4}$$

This relationship may be explained by a universal self-similarity in a topographic terrain of loess landforms. We also validated this relationship in the other two study areas. The empirical equation of segmentation threshold value *t* (Equation (4)) can be used to determine the segmentation threshold in areas of similar loess tableland landforms.
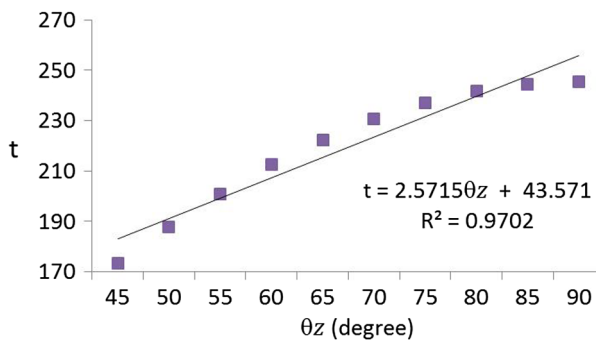

Figure 11. Scatter plot of the relationship between the segmentation threshold *t* and the zenith angle θ_z.
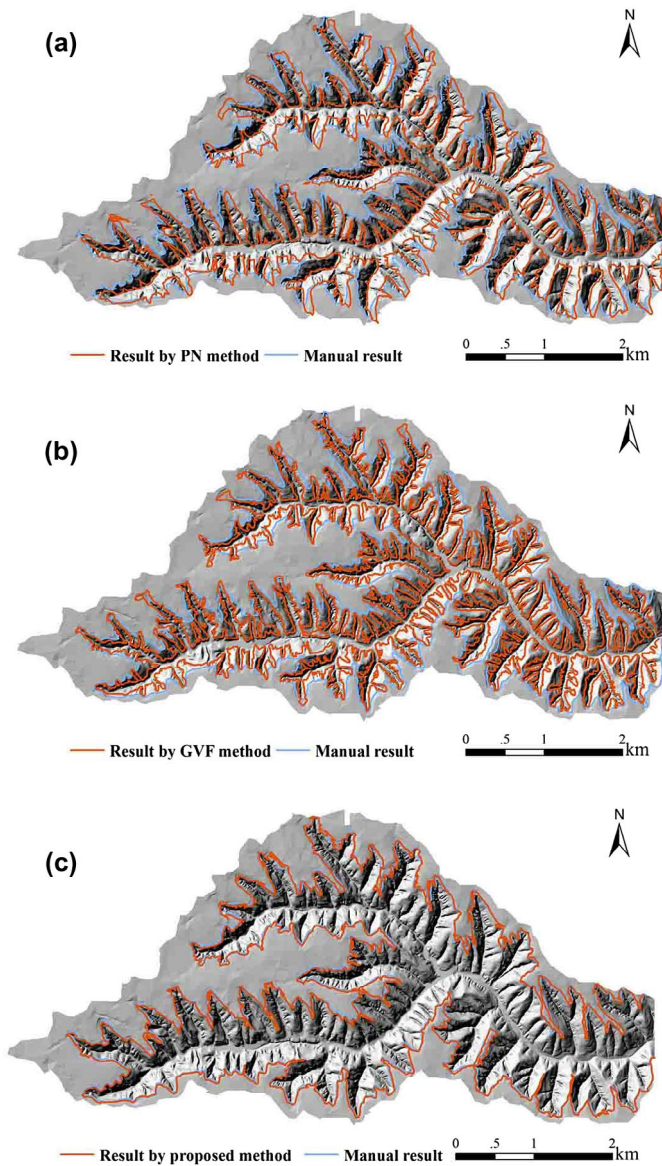
Figure 12. Extracted results of shoulder line from three methods: (a) P-N method, (b) GVF Snake method, and (c) BRS method.

Table 1. Frequency accumulation of EDOP with different distances.

Distance (*m*)	EDOP (%)		
	P-N method	GVF method	BRS method
10	67.6	68.2	64.8
20	81.2	90.6	89.7
30	90.5	94.6	93.4

Table 2. Computational efficiency of the three methods.

Methods	Time complexity	Run time (s)	$EDOP_{20}$ accuracy (%)
P-N method	O(kN)	7.6	81.2
BRS method	O(kN)	10.5	89.7
GVF method	O(NlgN)	290.6	90.6

Accuracy and efficiency

The methods discussed, including the P-N method (Tang et al., 2007), the GVF method (Song, 2013) and the BRS method, were compared with the reference data (Figure 12). The EDOP and its cumulative frequency of matching ratio were aggregately calculated with different error levels (Table 1). The result from Tang's method (Tang et al., 2007) are dense and complicated, whereas our results are more explicit and clear. This is because local gully details in lower height were shaded and then neglected by our method, allowing our result to reflect gully-affected area more clearly than Tang's method. Our BRS method achieved a high $EDOP_{20}$ accuracy, i.e. 89.77%, slightly lower than that of the GVF method but significantly higher than that of the P-N method (Table 1). It also showed that merely 7% of the errors from our BRS method are within 30 m, compared to nearly 10% for the P-N method.

Meanwhile, all three methods were applied to compare the efficiency of their performances. The performance environment had the following specifications: CPU Intel Core i7-4790 @ 3,600 GHz, 2 GB of memory, Windows 7 64-bit of operating system. The efficiency performances, listed in Table 2, showed that (1) although the run time of our BRS method and the P-N method were roughly similar, our BRS method demonstrated a significant improvement in terms of location accuracy; (2) although the GVF method performed better than the original Snake model (Yan et al., 2014), because of its parallelization, our BRS method is an improvement over the other methods because of the simplicity of the algorithm itself. Furthermore, when the DEM data size was quite large, performance of the GVF method could not increase further, whereas our BRS method could still perform well. Overall, our BRS method can achieve a high computational efficiency and an acceptable accuracy in a larger area. These differences can be of critical importance for practical use in soil and water conservation.

Conclusions

High temporal cost and low spatial accuracy in loess shoulder-line extraction have been critical issues in digital terrain analysis of the loess plateau areas, especially for geomorphological research and practical applications. The well-known hillshade model has been extensively applied for display enhancement. However, it has not been widely applied in extraction of terrain features. This paper proposed a relatively simple method for loess shoulder-line extraction based on the hillshade model.

Our experiment using 5-m DEMs in loess tableland areas led to the following conclusions. Our results showed that a fusion image of a bidirectional hillshade simulation contains sufficient information for extracting loess shoulder lines. Shoulder lines can be delineated by image segmentation. The zenith angle can be easily determined by a simple profile measurement, the azimuth angle has a weak influence on the accuracy, and the segmentation threshold can be determined by an empirical equation. The entire process can be

automatically completed with few manual interactions. Minor errors can also be eliminated automatically. Spatial accuracy of BRS method is better than that of the P-N method, and efficiency is better than that of the GVF method, although the accuracy is slightly lower, which achieves a good balance in terms of both accuracy and efficiency. Execution time for the production of a large DEM is significantly faster than for other methods in the same workstation. In addition, applicability of this method on other areas of loess tableland was confirmed. Although some limitations still exist in other landform types, we are optimistic about its potential applicability in other areas of both similar and different landform types.

ORCID

Jiaming Na http://orcid.org/0000-0002-6696-975X

References

Barbier, N., Proisy, C., Véga, C., Sabatier, D., & Couteron, P. (2011). Bidirectional texture function of high resolution optical images of tropical forest: An approach using LiDAR hillshade simulations. *Remote Sensing of Environment, 115*(1), 167–179.

Castillo, C., & Gómez, J. (2016). A century of gully erosion research: Urgency, complexity and study approaches. *Earth-Science Reviews, 160*, 300–319.

Chen, H., & Cai, Q. (2006). Impact of hillslope vegetation restoration on gully erosion induced sediment yield. *Science in China Series D: Earth Sciences, 49*(2), 176–192.

Chen, Y. G., Tang, G. A., Zhou, Y., Li, F. Y., Yan, S. J., & Zhang, L. (2012). The positive and negative terrain of loess plateau ectraction based on the multi-azimuth DEN shaded relief. *Scientia Geographica Sinica, 32*(01), 105–109.

Horn, B. K., & Schunck, B. G. (1981). Determining optical flow. In *1981 technical symposium east* (pp. 319–331). International Society for Optics and Photonics.

Jenks, G. F., & Caspall, F. C. (1971). Error on choroplethic maps: Definition, measurement, reduction. *Annals of the Association of American Geographers, 61*(2), 217–244.

Jiang, S., Tang, G., & Liu, K. (2015). A new extraction method of loess shoulder-line based on Marr-Hildreth operator and terrain mask. *PLOS ONE, 10*(4), e0123804.

Li, X. M., Wang, G., & Li, R. (2008). A DEM based method for extraction of valley shoulder line and slope heel line. *Bulletin of Soil and Water Conservation, 28*(01), 69–72.

Li, Z., Zhang, Y., Zhu, Q., He, Y., & Yao, W. (2015). Assessment of bank gully development and vegetation coverage on the Chinese Loess Plateau. *Geomorphology, 228*, 462–469.

Li, Z., Zhang, Y., Zhu, Q., Yang, S., Li, H., & Ma, H. (2017). A gully erosion assessment model for the Chinese Loess Plateau based on changes in gully length and area. *Catena, 148*, 195–203.

Liu, H., Deng, Q., Zhang, B., Li, X., Wang, L., Luo, M., & Qin, F. (2016). Influences of different surveying and mapping methods on fractal characteristics of gully-head shoulder lines. *Physical Geography, 37*(6), 387–408.

Lv, G. N., Qian, Y. D., & Chen, Z. M. (1998). Study of automated extraction of shoulder line of valley from grid digital elevation data. *Scientia Geographica Sinica, 18*(06), 567–573.

Noto, L. V., Bastola, S., Dialynas, Y. G., Arnone, E., & Bras, R. L. (2017). Integration of fuzzy logic and image analysis for the detection of gullies in the Calhoun Critical Zone Observatory using airborne LiDAR data. *ISPRS Journal of Photogrammetry and Remote Sensing, 126*, 209–224.

Poesen, J., Nachtergaele, J., Verstraeten, G., & Valentin, C. (2003). Gully erosion and environmental change: Importance and research needs. *Catena, 50*(2), 91–133.

Qiu, Y., Fu, B.-J., Wang, J., Chen, L., Meng, Q., & Zhang, Y. (2010). Spatial prediction of soil moisture content using multiple-linear regressions in a gully catchment of the Loess Plateau, China. *Journal of Arid Environments, 74*, 208–220.

Shruthi, R. B., Kerle, N., Jetten, V., Abdellah, L., & Machmach, I. (2015). Quantifying temporal changes in gully erosion areas with object oriented analysis. *Catena, 128*, 262–277.

Song, X., Tang, G., Li, F., Jiang, L., Zhou, Y., & Qian, K. (2013). Extraction of loess shoulder-line based on the parallel GVF snake model in the loess hilly area of China. *Computers & Geosciences, 52*(1), 11–20.

Tang, G. A., Xiao, C. C., Jia, D. X., & Yang, X. (2007). DEM based investigation of loess shoulder-line. In *Geoinformatics 2007* (Vol. 6753, pp. 12). International Society for Optics and Photonics.

Van Den Eeckhaut, M., Poesen, J., Verstraeten, G., Vanacker, V., Moeyersons, J., Nyssen, J., & Van Beek, L. (2005). The effectiveness of hillshade maps and expert knowledge in mapping old deep-seated landslides. *Geomorphology, 67*(3), 351–363.

Wang, K., Wang, C., Zhang, Q. F., & Ding, K. L. (2015). Loess shoulder line extraction based on openness and threshold segmentation. *Acta Geodartica et Cartographica Sinica, 44*(01), 67–75.

Wang, B., Zheng, F., Römkens, M. J., & Darboux, F. (2013). Soil erodibility for water erosion: A perspective and Chinese experiences. *Geomorphology, 187*, 1–10.

Yan, S. J., Tang, G. A., Li, F. Y., & Dong, Y. F. (2011). An edge detection based method for extraction of loess shoulder-line from grid DEM. *Geomatics and Information Science of Wuhan University, 36*(03), 363–367.

Yan, S., Tang, G., Li, F., & Zhang, L. (2014). Snake model for the extraction of loess shoulder-line from DEMs. *Journal of Mountain Science, 11*(6), 1552–1559.

Yoëli, P. (1967). The mechanisation of analytical hill shading. *The Cartographic Journal, 4*(2), 82–88.

Zhou, Y., Tang, G. A., Wang, C., Xiao, C. C., Dong, Y. F., & Sun, J. L. (2010). Automatic segmentation of loess positive and negative terrains based on high resolution grid DEMs. *Scientia Geographica Sinica, 30*(02), 261–266.

Zhou, Y., Tang, G. A., Xi, Y., & Tian, J. (2013). A shoulder-lines connection algorithm using improved Snake model. *Geomatics and Information Science of Wuhan University, 38*, 82–85.

Zhou, Y., Tang, G., Yang, X., Xiao, C., Zhang, Y., & Luo, M. (2010). Positive and negative terrains on northern Shaanxi Loess Plateau. *Journal of Geographical Sciences, 20*(1), 64–76.

Zhu, H. C., Tang, G. A., Zhang, Y. S., Yi, H. W., & Li, M. (2003). Thalweg in loess hill area based on DEM. *Bulletin of Soil and Water Conservation, 23*(05), 43–45+61.